

Trajectory Optimization for Coordinated Human-Robot Collaboration

Adam Fishman^{1,2} Chris Paxton¹, Wei Yang¹, Nathan Ratliff¹, and Dieter Fox^{1,2}

Abstract—Effective human-robot collaboration requires informed anticipation. The robot must simultaneously anticipate what the human will do and react both instantaneously and fluidly when its predictions are wrong. Even more, the robot must plan its own actions in a way that accounts for the human predictions but also with the knowledge that the human’s own behavior will change based on what the robot does. This back-and-forth game of prediction and planning is extremely difficult to model well using standard techniques. In this work, we exploit the duality between behavior prediction and control explored in the Inverse Optimal Control (IOC) literature to design a novel Model Predictive Control (MPC) algorithm that simultaneously plans the robot’s behavior and predicts the human’s behavior in a joint optimal control model. In the process, we develop a novel technique for bridging finite-horizon motion optimizers to the problem of spatially consistent continuous optimization using explicit sparse reward terms, *i.e.*, negative cost. We demonstrate the framework on a collection of cooperative human-robot handover experiments in both simulation and with a real-world handover scenario.

I. INTRODUCTION

Human behavior is determined by a diverse mixture of intent, world prediction, anticipation, physical limitations, and more. When planning in the presence of people, robotic decision processes often encapsulate these diverse desiderata under the lid of a black box dynamics function. When the robot and human’s goals are independent [1], [2], [3], this model has been very successful.

But, interaction and coordination on shared goals is substantially more complex. Modern robotics aims for human-robot collaboration beyond just safe co-existence, but with true, well-coordinated collaboration toward a unified goal. Encoding this intricate cooperative game into a naive dynamics function is challenging for the same reason directly predicting optimal actions without forward search or optimization is difficult [4], [5], [1]. Human collaborators, themselves, choose actions based on what they predict the robot will do in the same way we’d want the robot to choose good actions predicated on human predictions; predictions not only influence action choice, but are also influenced by the chosen actions.

In this paper, we study the ubiquitous and well-defined problem of human-robot handover [6], [7], [8], [9] as a representative example of coordinated interaction with shared goals. We design a novel optimal control technique that exploits the duality between control and prediction outlined in standard work on Inverse Optimal Control [10], [4], [5],

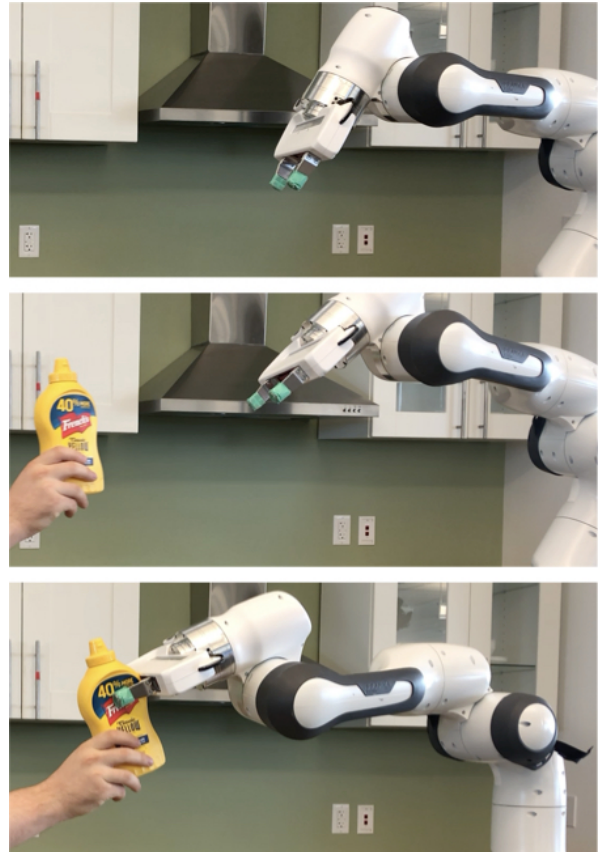


Fig. 1: Coordinating a fluid human-robot handover requires estimation of what the human is planning to do. Then, the robot can be in the right place to make the handover. By planning for both the human and the robot, we can achieve better and more natural human-robot collaborative motions in a variety of scenarios.

[1], [11], [12], wherein we model the human’s behavior as part of the optimal control problem. Our model moves beyond standard models of dynamics and assumes agency in the human’s choices, jointly optimizing over the robot’s actions and human predictions creating a bidirectional flow of information.

This combined human-robot system is fundamentally partially observable since the robot has no real control over the human and cannot directly observe factors influencing their decisions. Our planner must therefore, at a minimum, be reactive [13], which in this context means we must be able to re-optimize the solution in real time given each new observation within a Model-Predictive Control (MPC) paradigm [14]. Since speed is paramount, we adopt a modern motion optimization framework leveraging fast Gauss-Newton solvers [15], [16], [17] assuming relevant aspects

¹ NVIDIA {cpaxton, wyang, nratliff, dieterf}@nvidia.com

² University of Washington afishman@cs.washington.edu

of the human and robot are fully actuated. Additionally, to ensure spatial consistency of the resulting reactive behavior through re-optimizations, we introduce a novel class of explicit sparse reward terms, *i.e.*, negative costs, around the target which extend the target’s influence beyond the terminal potential to each intermediate time step enabling the system to intelligently trade off goal accumulation with smoothness criteria.

We evaluate our technique in both simulated ablation studies as well as real-world handover between a human participant and a Franka robot using a real-time vision-based perception system. We show that, especially in the presence of obstacles, our technique enables the robot to anticipate the human’s actions leading to well-coordinated, quick, and smooth handover behavior while timing the handover better than the alternatives, both quantitatively and qualitatively.

Our key contributions are: (1) A framework for jointly optimizing a robot’s actions and predicting human behavior assuming cooperative intent in a single optimization process. (2) A sparse reward framework for attaining spatial consistency of a continuously running finite-horizon MPC optimization process, enabling behavioral consistency across re-plans. (3) The use of this MPC process as a reactive MAP belief-space approximate POMDP solver [13] to accommodate the inherent uncertainty in the uncontrolled predictions of the human’s behavior.

Our video can be found at <https://fishy.ai/projects/tochrc>. We will also be open sourcing our code on the website.

II. RELATED WORK

Human behavior has been modeled successfully as an optimal (or soft-optimal) control process, but integrations into planners are typically uni-directional, with information flowing from prediction to planner, but not vice versa. For instance, [1] used predicted goal-oriented pedestrian behavior to augment navigation planners to minimize interaction, and [2] similarly modeled human reaching behaviors to reduce interaction or collision events while working along-side humans. Here we address coordination on shared goals, such as in human-robot handover, where bi-directional information flow modeling how the human reacts to robot action choices and vice versa becomes critical.

A key enabler of this work has been the progression of ideas in motion optimization resulting in modern approaches such as [17], [16], [15] which are both fast and expressive. Motion planning was first presented as an optimization problem in [18], and was sped up substantially in a quick progression of work [19], [20], [21]. These early optimizers addressed primarily the subproblem of smooth collision avoidance. The work of [22], [23], [16], extended the paradigm showing that generic second-order Gauss-Newton optimizers out-of-the-box could solve a more general class of constrained motion optimization problem, and soon thereafter, [15] demonstrated that standard factor graph tools could drastically simplify the modeling. We build on these ideas here, using a factor graph to model the problem and

fast modern optimizers to solve the continuous optimization loop in real time.

While our setting is fundamentally partially observable, we do not address the POMDP problem directly, other than to use standard reactive MAP approximation techniques of [13] to motivate the importance of continuous re-optimization, which becomes possible given the advances in modern motion optimization research mentioned above. To achieve better reactivity, a full system implementation would leverage real-time reactive motion generation techniques such as Riemannian Motion Policies (RMPs) [24], [25] as well, but the primary bottleneck of the proposed technique is the real-time MPC loop, so this work focuses entirely on that latter process.

Finally, human-robot handover itself is well-studied. Much of this work analyzes the formulation of the human handover and how to structure the action naturally [6], [7]. Our method applies more specifically to the approach phase of the handover as our optimization can produce smooth, adaptive, and coordinated task-space trajectories. Related ideas include [26] who exploit a database of human demonstrations to produce natural and fluid plans. Likewise, [8] uses imitation learning to mimic human behavior and [9] uses a human-inspired dynamics controller to model the entire action: approach, grasp, retract. These methods are well-suited for controlled interaction settings, but generalizing them to handle the diversity of speed and environmental variations encountered in the real world is challenging.

III. FINITE-HORIZON OPTIMIZATION FOR HUMAN-ROBOT COORDINATION

In this section, we present how to formulate the handover task as an optimization problem with a finite time horizon. We will discuss how to relax the finite-horizon constraint with a novel distance-based reward function in Section IV.

A. Overall Optimization Structure

When interacting with an uncontrolled agent A (*e.g.*, human) for the handover task, the robot R needs to plan a trajectory $\xi^R = \{\mathbf{q}_i^R\}_{i=0}^T$ to reach out the agent, where \mathbf{q}_i^R is a time-indexed position in the robot’s configuration space. Moreover, the robot needs to also estimate the present state and the future action of the agent. In this paper, we assume that the agent A acts with reasonable intent. Therefore, at any given time t , we can model the agent’s intent as an optimal trajectory ξ^A with a random noise ϵ_A under this cooperative assumption.

To search for the optimal ξ^R and ξ^A in a fixed number of steps, we optimize the following cost function,

$$C(\xi^R, \xi^A) = \lambda \cdot (c(\xi^R), c(\xi^A), c(\xi^R, \xi^A)), \quad (1)$$

where $c(\xi^R)$, $c(\xi^A)$ and $c(\xi^R, \xi^A)$ model the objective for optimal trajectories of the robot, the agent, and the robot-agent collaboration, respectively. λ is a vector of weights on each individual cost function and is set empirically.

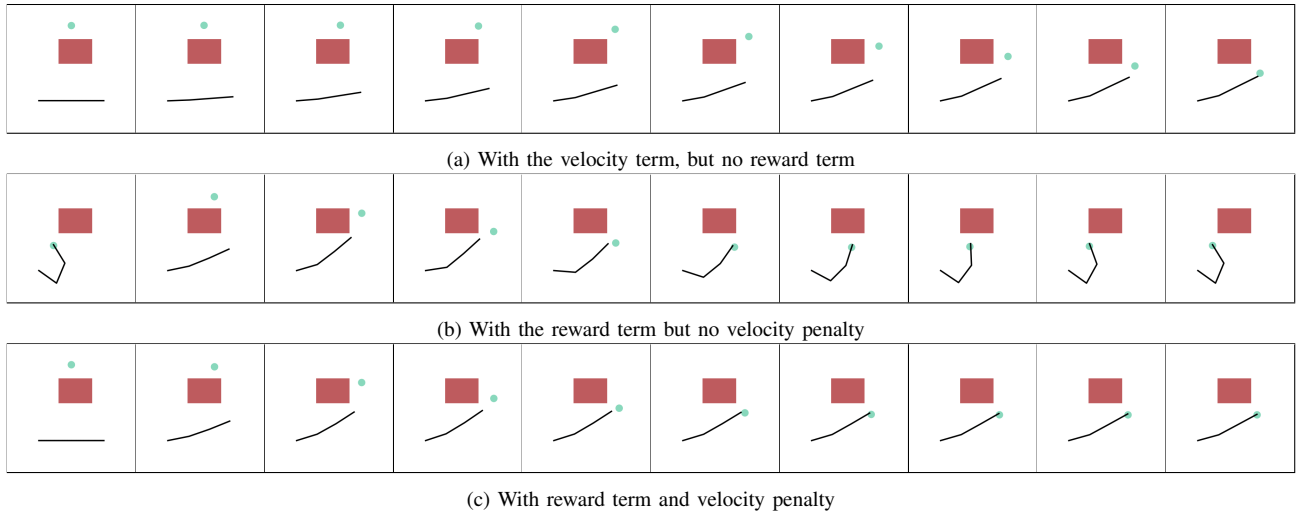


Fig. 2: With the reward term imposed, our planner pushes the two agents to each other faster than without as a function of their distance. By including the reward term, we are able to run our planner with a fixed time horizon. As the agents get closer with each MPC step, they converge to each other in less time. This allows us to avoid an exponential slow-down while using a fixed time horizon.

B. Modeling the robot

First, we define the cost modeling the robot trajectory,

$$c(\xi^R) = \sum_{i=0}^T c_i(\mathbf{q}_i^R, \dot{\mathbf{q}}_i^R, \ddot{\mathbf{q}}_i^R), \quad (2)$$

where T is the total number of time steps and \mathbf{q}^R , $\dot{\mathbf{q}}^R$, $\ddot{\mathbf{q}}^R$ are the position, velocity, and acceleration of the joints of the robot in configuration space. In what follows, we will also use $\mathbf{x}_i^R = \phi(\mathbf{q}_i^R) = [\mathbf{R}_i^R, \mathbf{p}_i^R]$ to represent the 6-DOF pose of the end effector in the world frame, after applying the forward kinematics function $\phi(\cdot)$.

Equation 2 can be split into the sum of individual cost functions, which we define in what follows

Obstacle avoidance and joint constraints. To prevent hitting the joint limits and to avoid obstacles, we include three cost functions $c_{\text{joint}}(\mathbf{q}_i^R)$, $c_{\text{joint}}(\dot{\mathbf{q}}_i^R)$, and $c_{\text{obs}}(\mathbf{q}_i^R)$.

Let J denote the indices of the joints, θ_j^R denote the angle of j th joint, and $(\theta_{j, \min}^R, \theta_{j, \max}^R)$ denote the corresponding joint limitation, we employ a hinge-loss based cost [27] for the joint limit:

$$c_{\text{joint}}(\mathbf{q}_i^R) = \sum_{j \in J} \|c(\theta_j^R)\|^2, \quad (3)$$

where $c(\theta_j^R)$ is defined as

$$c(\theta_j^R) = \begin{cases} -\theta_j^R + \theta_{j, \min}^R - \epsilon_j, & \text{if } \theta_j^R < \theta_{j, \min}^R + \epsilon_j \\ 0, & \text{if } \theta_{j, \min}^R \leq \theta_j^R \leq \theta_{j, \max}^R \\ \theta_j^R - \theta_{j, \max}^R + \epsilon_j, & \text{if } \theta_j^R > \theta_{j, \max}^R - \epsilon_j \end{cases} \quad (4)$$

Here ϵ_j is the joint limit error tolerance for joint j .

We also impose a cost

$$c_{\text{joint}}(\dot{\mathbf{q}}_i^R) = \sum_{j \in J} \|c(\dot{\theta}_j^R)\|^2, \quad (5)$$

where $c(\dot{\theta}_i^R)$ is formulated similarly to Equation 4 using $\dot{\theta}$ in place of θ .

We assume that the environment is static, *i.e.*, the camera and the obstacles are unchanging. We first pre-compute a

signed distance function representation of the environment. Then, as in [18], we use a sphere-based “skeleton” that covers the robot’s entire volume and surface area. The spheres allow for a sparse and efficient representation of the robot’s volume. Our total obstacle cost is then the sum of the cost at each sphere:

$$c_{\text{obs}}(\mathbf{q}_i^R) = \sum_{s \in \text{spheres}} \|c(s)\|^2, \quad (6)$$

where

$$c(s) = \begin{cases} -d_s + s_{\text{radius}}, & \text{if } d_s \leq s_{\text{radius}} \\ 0, & \text{if } d_s > s_{\text{radius}} \end{cases} \quad (7)$$

Here d_s is the value of the signed distance function at the sphere s ’s center.

Velocity and acceleration constraints. We include independent constraints for configuration-space velocity and acceleration constraints, $c_i(\dot{\mathbf{q}}^R)$ and $c_i(\ddot{\mathbf{q}}^R)$, that each constrain these values to be zero. The velocity penalty ensures that the robot slows after reaching its goal, while the acceleration penalty ensures the robot moves fluidly without overshooting its target. Due to software limitations, we also add an additional velocity constraint, which we describe in Section V.

End effector constraints. We also constrain the robot’s end effector orientation to match an optimal value and add this to our overall cost function. In the 2D case, this optimal value is straightforward: the robot should always be oriented towards the human. The optimal 3D orientation is more complex.

Let G denote the coordinate frame of the gripper where the z -axis \mathbf{z}_G points directly out from the gripper and the x -axis \mathbf{x}_G points down perpendicular to gripper. When the gripper is perfectly flat, \mathbf{x}_G points straight down to the ground. We wish to align \mathbf{z}_G with \mathbf{v} , the ray from the end effector to the human’s hand. We also want the end effector to be more-or-less flat. So, assuming the world frame has \mathbf{z}_W up, we want to find \mathbf{x}_G that when expressed in the world coordinates, has

the lowest \mathbf{z} coordinate, *i.e.*, in the world frame,

$$0 = \mathbf{z}_G \cdot \mathbf{x}_G = \frac{\mathbf{v}}{\|\mathbf{v}\|} \cdot [x_{\mathbf{x}_G}, y_{\mathbf{x}_G}, z_{\mathbf{x}_G}], \quad (8)$$

where $[x_{\mathbf{x}_G}, y_{\mathbf{x}_G}, z_{\mathbf{x}_G}]$ correspond to the world frame coordinates of $[1, 0, 0]_G$ in the gripper frame. We also know $x_{\mathbf{x}_G} = 1 - \sqrt{y_{\mathbf{x}_G}^2 + z_{\mathbf{x}_G}^2}$.

If the gripper does not point straight up, we can first solve for $z_{\mathbf{x}_G}$, then take the derivative with respect to $y_{\mathbf{x}_G}$ and set it to zero in order to find the \mathbf{x}_G that points most-down. Then, $\mathbf{y}_G = \mathbf{z}_G \times \mathbf{x}_G$ and we can use these three axes to construct our desired rotation matrix $\hat{\mathbf{R}}$.

With $\hat{\mathbf{R}}$, we use the same cost function from [28] to constrain the robot to face this direction.

$$c(\mathbf{R}_i^R) = \log(\hat{\mathbf{R}}^{-1} \mathbf{R}_i^R)^\vee$$

where $\log(\cdot)$ is the logarithmic map and \vee is the operator that takes a skew-symmetric matrix to a vector.

As a simplifying assumption to improve planning efficiency, we only compute $\hat{\mathbf{R}}$ once at each planning cycle using current observation of both the robot and agent. Since we run many iterations closed-loop, the robot will continue to face towards the human's position.

C. Modeling the uncontrolled agent

We model the uncontrolled agent as a second robot with a known starting pose. Therefore, the cost function

$$c(\xi^A) = \sum_{i=0}^T c(\mathbf{q}_i^A, \dot{\mathbf{q}}_i^A, \ddot{\mathbf{q}}_i^A) \quad (9)$$

with the same constituent cost functions as used for the robot.

In our implementation, however, we ignore several of these constraints due to system limitations. We discuss this more in Section V.

D. Modeling the robot-agent collaboration

At the end of the trajectory, the robot and the uncontrolled agent should meet with each other. To do this, we enforce their end effector positions to be as close to each other as possible,

$$c(\xi^R, \xi^A) = c(\mathbf{p}_T^R, \mathbf{p}_T^A) = \|\mathbf{p}_T^R - \mathbf{p}_T^A\|^2 \quad (10)$$

E. Optimization

Each term in the cost function (1) is an $L2$ penalty. Therefore it can be phrased as a nonlinear least squares optimization. Following [29] and [15], we use Gauss-Newton to optimize our cost. Gauss-Newton has no convergence guarantee[30], but as shown in [29], the performance is similar to Newton's method, which has guaranteed local convergence. Experimentally, we found our optimization to converge nearly 100% of the time, even in the presence of sensor noise. See Table II for our convergence metrics under suboptimal sensor conditions.

Fig. 3: The distance-based reward function $1 - e^{-\frac{\|\mathbf{x}_i^R - \mathbf{x}_i^A\|^2}{2\sigma^2}}$ added to each time step $0 < i < T$

IV. SPATIALLY CONSISTENT INTERACTION USING EXPLICIT TARGET REWARDS

When two agents collaborate without explicit synchronization, their interaction and behavior should be a function of state and not tied to a specific clock. For example, in a handover, we infer the dynamics of our partner and try to smoothly match them, if we're moving too fast we slow down, and if we're moving too slow we speed up. Likewise, when grasping an object from a conveyor belt or from a moving vehicle, we do so by directly coordinating state (distance and motion); the policy is primarily a function of the combined human-robot state and in many cases, does not not explicitly depend on time. We seek to mimic this state dependent behavior with our robot's policy.

As is typical in Model Predictive Control, we account for deviations from the planner's output by continually re-optimizing with a fixed-time horizon at each successive time step. However, as the two agents approach each other, the fixed horizon becomes a bottleneck.

Suppose at the beginning, the approximate distance between the two agents is d and they need to meet each other in T time steps, then the average speed is $\frac{d}{T}$. At the second time step, it would be $(\frac{T-1}{T}) \frac{d}{T}$, followed by $(\frac{T-1}{T})^2 \frac{d}{T}$ at the third step, etc. The exponential decay causes the two agents to stop before reaching each other.

We counteract the slowdown by adding a distance based reward term weighted by λ_{reward} to the robot-agent collaboration cost defined in Eq. (10) at every point on the trajectory.

$$c(\xi^R, \xi^A) = c(\mathbf{p}_T^R, \mathbf{p}_T^A) + \lambda_{\text{reward}} \sum_{i=0}^T r(\mathbf{p}_i^R, \mathbf{p}_i^A), \quad (11)$$

where the reward $r(\mathbf{p}_i^R, \mathbf{p}_i^A)$ at step i is defined as

$$r(\mathbf{p}_i^R, \mathbf{p}_i^A) = 1 - e^{-\frac{\|\mathbf{p}_i^R - \mathbf{p}_i^A\|^2}{2\sigma^2}}. \quad (12)$$

This reward is motivated by the types of sparse rewards used in reinforcement learning [31]. Since our goal is to minimize cost, reward can be viewed as negative cost. Such a reward can be modeled as an upside down radial basis function over the distance between the robot's end-effector and the interacting agent, *i.e.*, zero when the two are far from each other and increasing (negatively) once they are very close. This rewards the robot for getting within touching distance of the interacting agent (and similar with the agent), but does not penalize the pair for having to be far from each other earlier in the trajectory due to competing smoothness criteria. Since we have a fixed finite-horizon, without loss of generalization, we can shift each of these reward terms up by a constant so its minimum value is zero as given in the equation.

With this shift upward, our formulation of the reward term becomes identical to the Welsch robust estimator [32].

Although the reward is not a quadratic cost, solving for the local minimum is equivalent to solving for

$$\|\mathbf{t}_i^R - \mathbf{t}_i^A\|^2 e^{-\frac{\|\mathbf{t}_i^R - \mathbf{t}_i^A\|^2}{2\sigma^2}} \quad (13)$$

using iteratively reweighted least-squares [33].

As shown in Figure 2, with the reward term imposed, the two end effectors reach each other faster than without. However, due to the acceleration penalty, we observe the two arms colliding and then moving erratically in order to maintain their velocity and the reward. To counteract this, we add a velocity penalty that brings them both to a stop after they intersect.

V. IMPLEMENTATION DETAILS

Much as in [15], we phrase our optimization task as a factor-graph based optimization. We did this in order to exploit the fast optimization software tools from GTSAM [34]. The cost functions required by GTSAM are typically phrased as a Mahalanobis distance, i.e. $\|\mathbf{v}\|_{\Sigma} = \mathbf{v}^T \Sigma^{-1} \mathbf{v}$. However, unlike their implementation, our optimization is not phrased on probabilistic inference. Instead, we exclusively use isotropic covariances, i.e. diagonal covariance matrices where the variance on every dimension is the same. The λ weight for each cost function in our formulation is then equal to $1/\sigma^2$ in the covariance matrix.

We are able to run our algorithm to perform a human handover in real time on a Franka Emika Panda arm. In order to obtain the human’s pose, we used the Microsoft Azure Kinect DK and its included body tracking SDK.

At the time of submission, the Azure body tracking SDK provides position but not orientation for the wrist. Because the human is cooperative, we assume they will orient the handover object in a graspable position for the robot. As such, we do not impose any orientation based costs on the human pose estimate and instead rely on our cost term for the robot’s end effect orientation.

On a workstation with an 3.4ghz Intel® Core™ i7 and 32GB of RAM running Ubuntu 18.04, we obtained poses at a rate of 30hz. We use DART [35] to calibrate the robot configuration into the Azure frame. We then are able to obtain starting positions for the human and robot at each optimization step.

GTSAM has limited support for hard constraints, so following [15], we modeled the robot and human’s starting positions as soft constraints with very high weights. Also following [15], we used a soft constraint to model velocity by adding a highly weighted cost function of the form $\|\dot{\mathbf{q}}_i - (\mathbf{q}_{i+1} - \mathbf{q}_i)\|^2$.

We run both our optimizer and DART on the same workstation running Ubuntu 16.04 and equipped with an 3.7ghz Intel® Core™ and 32GB of RAM. We obtain DART’s positional estimates at 10hz, and we are able to run our optimizer with Levenberg-Marquardt between 7hz and 8hz.

When the Franka is within a minimum threshold—we used 10cm—it engages the gripper and tries to grasp the object. If it misses and closes all the way, the gripper re-opens and

the planner resumes trying to engage in the handover until it succeeds. We found the robot to miss the handover when the human moves too quickly for the body tracker to maintain a stable estimate.

VI. EXPERIMENTS

In this section we aim to answer the following questions about our proposed algorithm: 1) How do our method’s generated trajectories compare to those produced by baseline methods? 2) How robust is our algorithm to noisy sensors? 3) Can our proposed method be used in a real world setting?

TABLE I: Algorithmic benchmarks (\uparrow denotes higher is better and \downarrow denotes lower is better): our algorithm is best able to approximate the timing of the uncontrolled agent. The attractor-based algorithm produces trajectories with significantly greater acceleration and jerk than both the robot-only and our algorithm. The robot-only algorithm outperforms ours in reducing acceleration and jerk, but does this by waiting for the uncontrolled agent to become visible and then moving, leading to significantly longer trajectories.

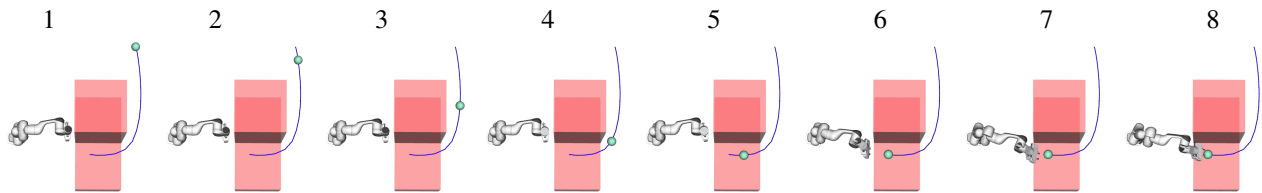
Metric		Robot only	Attractor	Ours
Success rate (%)	\uparrow	100	94	100
Trajectory Length Error	\downarrow	0.21 ± 0.19	0.24 ± 0.24	0.11 ± 0.18
Acceleration (cm/s^2)	\downarrow	1.42 ± 0.22	3.31 ± 1.42	2.05 ± 0.57
Jerk μ (cm/s^3)	\downarrow	1.62 ± 0.41	3.84 ± 1.76	2.42 ± 0.72

Our algorithm predicts the motion and dynamics of the uncontrolled agent and reacts accordingly. In order to evaluate each component, we benchmarked our algorithm against two different baselines

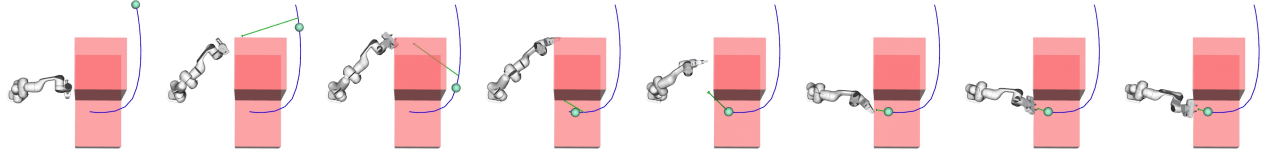
- **Robot only:** A planner that only accounts for the Euclidean position of the uncontrolled agent. At each time step, the robot optimizes a trajectory around any obstacles to match its end effector position with the other agent’s end effector position.
- **Attractor:** A planner that applies an attractor based policy to both end effectors. This policy assumes the two arms will move toward each other at each time step. When obstacles are present, they act as repellant forces, opposing the attracting force. We implemented this method by using our same algorithm with a very short time horizon, i.e., $T = 5$, which is the shortest trajectory supported by our low-level controller.

Our simulated environment is shown in Figure 4. The robot and uncontrolled agent start on opposite sides of an obstacle. To evaluate the algorithms without bias, we independently planned the uncontrolled trajectory to go from a randomized location on the opposing side of the obstacle to a randomized point in the robot’s reachable space, while also avoiding the obstacles. We do this by minimizing our same velocity, obstacle-avoidance, and acceleration costs for the hand, while also adding a cost term with high λ to constrain the hand to our randomly chosen start and end positions, as in [15]. These trajectories range from 12-16 time steps.

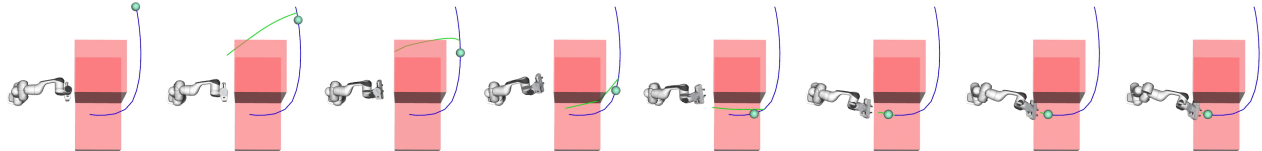
We then replayed the uncontrolled trajectory where at the end, the agent waits for the robot. We modeled the agent as a ball with a 10cm radius and as such, we considered a trial to be successful if the robot was able to plan a trajectory



(a) **Robot only** The robot waits to move until frame 6 when it has an unobstructed path to the agent. The robot is slow to react to the agent.



(b) **Attractor** This strategy estimates the agent will move directly toward the robot, as shown with the green arrow. It produces very reactive trajectories with high acceleration and jerk. At frame 2, the robot swings fully to one side of the obstacle, and during frames 5-7, it swings back.



(c) **Ours** Our method estimates a full trajectory for the uncontrolled agent, as represented by the green line. In frame 4, the robot moves slightly to the left, but then in frames 5-7 smoothly moves to the right side of the obstacle. This path change happens as the homotopy class of the agent's trajectory around the obstacle becomes clear.

Fig. 4: Our bench-marking setup. We model the uncontrolled agent as a floating sphere and give it a randomized starting position on the opposing side of the obstacle from the robot. We then plan a trajectory to a randomized point in the robot's reachable space, represented by the blue line. We use this trajectory to compare the three different algorithms. Our quantitative metrics are in Table I.

TABLE II: Robustness metrics: we evaluate our robustness to measurement noise by determining, for a given amount of measurement noise, the percentage of handovers that can be completed within twice the time of the uncontrolled trajectory

Error σ (cm)	2	5	7	10	15
% Successful	100	100	92	90	50

where its end effector was within 10cm of the agent in under twice the uncontrolled trajectory length.

We ran 50 trials, where compared the three algorithms with the same randomized trajectory. We adopt four different metrics, *i.e.*, *Success rate*, *trajectory length error*, *acceleration*, and *jerk*, for evaluation. We define the *trajectory length error* as $|1 - T_{\text{success}}/T_{\text{uncontrolled}}|$ where T_{success} is the time it takes to finish a successful action and $T_{\text{uncontrolled}}$ is the length of the uncontrolled trajectory. The quantitative results are shown in Table I.

Both qualitatively and quantitatively, we saw the *attractor* algorithm leads the robot to jerk heavily when the agent's path around the obstacle is non-obvious. Meanwhile, the *robot-only* planner tends to wait to move until the path around the obstacle is unobstructed, leading it to take longer to reach the agent. Our algorithm is able to smoothly predict the agents path. We also saw our algorithm produces lower *trajectory length error* that the others—meaning our algorithm is better able to match the length of the uncontrolled trajectory. See our video for a demonstration.

We also evaluated our algorithm's robustness to measurement noise. In our real-robot experiments, we observed that our planner failed when the calibration and/or body tracker were misaligned. To measure this, we planned a randomized uncontrolled trajectory in the same fashion as before. However, we introduced Gaussian noise with increasing σ into the

robot's perception of the trajectory. We then measured how often the robot could intersect the agent at its *actual* location within twice the uncontrolled trajectory length. Results with varying σ are in Table II.

As shown in Figure 1, we are able to run our algorithm on a real robot using the setup described in Section V. See our video for more examples.

VII. CONCLUSION

We described an MPC approach that simultaneously optimizes motion plans for both a robot and an (uncontrolled) human in order to enable coordination on cooperative tasks, with an application to human-robot handovers in obstacle-rich environments. In the future, we will apply our work to other coordination problems that have been explored in the literature, such as motion in a crowd [3] and camera control [36], [37].

VIII. ACKNOWLEDGEMENTS

We would like to thank Alexander Lambert, Asif Rana, Byron Boots, Stuart Anderson, and Mustafa Mukadam for their helpful discussions and feedback on this project. We would also like to thank Mustafa Mukadam, Jing Dong, as well as the GTSAM community, for their open source code, which we used as the foundation of our code base.

REFERENCES

- [1] B. D. Ziebart, N. Ratliff, G. Gallagher, C. Mertz, K. Peterson, J. A. D. Bagnell, M. Hebert, A. Dey, and S. Srinivasa, "Planning-based prediction for pedestrians," in *IROS*, 2009.
- [2] J. Mainprice, R. Hayne, and D. Berenson, "Goal set inverse optimal control and iterative re-planning for predicting human reaching motions in shared workspaces," *IEEE Transaction on Robotics (TRO)*, 2016.

- [3] H. Bai, S. Cai, N. Ye, D. Hsu, and W. S. Lee, "Intention-aware online pomdp planning for autonomous driving in a crowd," in *2015 IEEE international conference on robotics and automation (ICRA)*. IEEE, 2015, pp. 454–460.
- [4] N. Ratliff, D. Silver, and J. A. D. Bagnell, "Learning to search: Functional gradient techniques for imitation learning," *Autonomous Robots*, vol. 27, no. 1, pp. 25–53, July 2009.
- [5] B. D. Ziebart, A. Maas, J. A. Bagnell, and A. K. Dey, "Human behavior modeling with maximum entropy inverse optimal control," in *AAAI Spring Symposium on Human Behavior Modeling*, 2009.
- [6] K. Strabala, M. K. Lee, A. D. Dragan, J. Forlizzi, S. S. Srinivasa, M. Cakmak, and V. Micelli, "Toward seamless human-robot handovers," in *HRI 2013*, 2013.
- [7] C.-M. Huang, M. Cakmak, and B. Mutlu, "Adaptive coordination strategies for human-robot handovers," in *Robotics: Science and Systems*, 2015.
- [8] G. Maeda, G. Neumann, M. Ewerton, R. Lioutikov, O. Kroemer, and J. Peters, "Probabilistic movement primitives for coordination of multiple humanrobot collaborative tasks," *Autonomous Robots*, vol. 41, pp. 593–612, 2017.
- [9] J. R. Medina, F. Duvallat, M. Karnam, and A. Billard, "A human-inspired controller for fluid human-robot handovers," *2016 IEEE-RAS 16th International Conference on Humanoid Robots (Humanoids)*, pp. 324–331, 2016.
- [10] A. Y. Ng and S. J. Russell, "Algorithms for inverse reinforcement learning," in *International Conference on Machine Learning (ICML)*, 2000.
- [11] K. Dvijotham and E. Todorov, "Inverse optimal control with linearly-solvable mdps," in *In International Conference on Machine Learning*, 2010.
- [12] S. Levine and V. Koltun, "Continuous inverse optimal control with locally optimal examples," in *ICML 2012*, 2012.
- [13] K. Murphy, "A survey of pomdp solution techniques," *Environment*, vol. 2, 10 2000.
- [14] T. Erez, K. Lowrey, Y. Tassa, V. Kumar, S. Koley, and E. Todorov, "An integrated system for real-time model-predictive control of humanoid robots," in *IEEE/RAS International Conference on Humanoid Robots*, 2013.
- [15] M. Mukadam, J. Dong, X. Yan, F. Dellaert, and B. Boots, "Continuous-time Gaussian process motion planning via probabilistic inference," *International Journal of Robotics Research*, vol. 37, no. 11, pp. 1319–1340, 7 2018. [Online]. Available: <http://arxiv.org/abs/1707.07383http://dx.doi.org/10.1177/0278364918790369>
- [16] N. Ratliff, M. Toussaint, and S. Schaal, "Understanding the geometry of workspace obstacles in motion optimization," in *IEEE International Conference on Robotics and Automation (ICRA)*, 2015.
- [17] M. Toussaint, "A tutorial on Newton methods for constrained trajectory optimization and relations to SLAM, Gaussian Process smoothing, optimal control, and probabilistic inference," in *Geometric and Numerical Foundations of Movements*, J.-P. Laumond, Ed. Springer, 2017.
- [18] N. Ratliff, M. Zucker, J. A. Bagnell, and S. Srinivasa, "CHOMP: Gradient optimization techniques for efficient motion planning," 2009.
- [19] M. Kalakrishnan, S. Chitta, E. Theodorou, P. Pastor, and S. Schaal, "Stomp: Stochastic trajectory optimization for motion planning," in *2011 IEEE International Conference on Robotics and Automation*, May 2011, pp. 4569–4574.
- [20] J. P. Chonhyon Park and D. Manocha, "ITOMP: Incremental trajectory optimization for real-time replanning in dynamic environments," in *International Conference on Automated Planning and Scheduling (ICAPS)*, 2012.
- [21] J. Schulman, J. Ho, A. Lee, I. Awwal, H. Bradlow, and P. Abbeel, "Finding locally optimal, collision-free trajectories with sequential convex optimization," 06 2013.
- [22] M. Toussaint, "Robot trajectory optimization using approximate inference," in *ICML*, 2009, pp. 1049–1056.
- [23] —, "Newton methods for k-order Markov Constrained Motion Problems," 7 2014. [Online]. Available: <http://arxiv.org/abs/1407.0414>
- [24] N. D. Ratliff, J. Issac, D. Kappler, S. Birchfield, and D. Fox, "Riemannian motion policies," *arXiv preprint arXiv:1801.02854*, 2018.
- [25] C.-A. Cheng, M. Mukadam, J. Issac, S. Birchfield, D. Fox, B. Boots, and N. Ratliff, "Rmpflow: A computational graph for automatic motion policy generation," *arXiv preprint arXiv:1811.07049*, 2018.
- [26] K. Yamane, M. Revfi, and T. Asfour, "Synthesizing object receiving motions of humanoid robots with human motion database," *2013 IEEE International Conference on Robotics and Automation*, pp. 1629–1636, 2013.
- [27] M. Mukadam, X. Yan, and B. Boots, "Gaussian Process Motion planning," in *Proceedings - IEEE International Conference on Robotics and Automation*, vol. 2016-June. Institute of Electrical and Electronics Engineers Inc., 6 2016, pp. 9–15.
- [28] J. Dong, B. Boots, and F. Dellaert, "Sparse Gaussian processes for continuous-time trajectory estimation on matrix Lie groups," *Arxiv*, vol. abs/1705.06020, 2017. [Online]. Available: <http://arxiv.org/abs/1705.06020>
- [29] N. D. Ratliff, M. Toussaint, J. Bohg, and S. Schaal, "On the fundamental importance of gauss-newton in motion optimization," *Arxiv*, vol. abs/1605.09296, 2016.
- [30] W. F. Mascarenhas, "The divergence of the bfgs and gauss newton methods," 2013.
- [31] M. Riedmiller, R. Hafner, T. Lampe, M. Neunert, J. Degraeve, T. van de Wiele, V. Mnih, N. Heess, and J. T. Springenberg, "Learning by playing solving sparse reward tasks from scratch," in *Proceedings of the 35th International Conference on Machine Learning*, ser. Proceedings of Machine Learning Research, J. Dy and A. Krause, Eds., vol. 80. Stockholmsmssan, Stockholm Sweden: PMLR, 10–15 Jul 2018, pp. 4344–4353. [Online]. Available: <http://proceedings.mlr.press/v80/riedmiller18a.html>
- [32] P. W. Holland and R. E. Welsch, "Robust regression using iteratively reweighted least-squares," 1977.
- [33] Z. Zhang, "Parameter estimation techniques: a tutorial with application to conic fitting," *Image Vision Comput.*, vol. 15, pp. 59–76, 1997.
- [34] F. Dellaert and M. Kaess, "Factor Graphs for Robot Perception," *Foundations and Trends in Robotics*, vol. 6, no. 1-2, pp. 1–139, 2017.
- [35] T. Schmidt, R. A. Newcombe, and D. Fox, "DART: Dense articulated real-time tracking," in *Robotics: Science and Systems*, 2014.
- [36] D. Rakita, B. Mutlu, and M. Gleicher, "An autonomous dynamic camera method for effective remote teleoperation," in *Proceedings of the 2018 ACM/IEEE International Conference on Human-Robot Interaction*. ACM, 2018, pp. 325–333.
- [37] R. Bonatti, C. Ho, W. Wang, S. Choudhury, and S. A. Scherer, "Towards a robust aerial cinematography platform: Localizing and tracking moving targets in unstructured environments," in *IEEE/RSJ International Conference on Intelligent Robots and Systems (IROS)*, 2019.